Synthesis and Properties of Nanocomposites

By *Dieter Vollath*,* and *Dorothée V. Szabó*

Nanocomposites may exhibit new properties of technical interest. Technical applications require many particles, leading to interaction of the particles thwarting the performance of these materials. To exploit specific nano properties, the use of composites preventing the particles from interaction is necessary. This leads to the application of nanocomposites. The most homogeneous composites consist of a core coated with an outer layer of a second ceramic or a polymer. For industrial or at least semi industrial production of nanocomposites, a process leading to non agglomerated powders in a sufficient quantity is needed. Additionally, coating of the particles with either a second ceramic phase or an organic one is necessary. The Karlsruhe Microwave Plasma Process fulfils these conditions.

1. Introduction

Nanomaterials are defined as materials with grain sizes below 100 °nm or more stringent, as materials with special properties depending on their small grain size, restricting in many cases -nanomaterials to grain sizes below 10 nm. Many crystallised or amorphous nanomaterials exhibit interesting physical properties.[1] These properties may be related to the large amount of grain boundaries in the materials, or to the special electronic structure of the small particles. In the latter case, the special properties are ones of single isolated particles that are lost if the particles interact. To avoid interaction between the particles they have to be kept in a certain distance depending on the type of interaction. Prevention of tunnelling between the particles needs less distance as compared to dipole interaction.

These considerations lead to nanocomposites consisting of an active phase, carrying the special physical property and a passive one, acting as distance holder. It is essential for nanocomposites that no one of the active particles touches a second active one. Additionally, the amount of the second phase should be small. These nearly contradicting demands cannot be met with a production process based on mechanical blending of the active and the distance holder phase. Only a process that coats particles produced in a first step with the second phase leads to a product with the necessary uniformity.[2] The Karlsruhe Microwave Plasma Process for the synthesis of nanocrystalline ceramic powders solved these problems for the first time.[2–7] The main characteristics of this process are low reaction temperature and conditions for synthesis avoiding particle agglomeration in combination with relatively high production rates. The reaction temperature is low, because the reactants are dissociated or ionised in the microwave plasma; therefore, thermal activation of the chemical reactions is not necessary. Particle agglomeration is avoided, because the particles leave the reaction zone with electric charges of equal sign. Therefore, they repel each other. This allows coating of the particles in a second step with either a second ceramic phase or a polymer layer.[2,7,8] Later, a more conventional variation of this process for ceramic coating applying a tubular furnace was developed.[9] Generally, this process needs reaction temperatures above 1000 °C to overcome kinetic obstacles of the chemical reactions and to increase the reaction rate. As the particles in general are not repelling each other, this process forms clustered particles; therefore, applying this process leads to some extend to coated clusters. Earlier attempts by Hung and Katz to produce mixed oxide powders nanoparticles of the core/shell type by flame synthesis.[10,11] lead to coated clusters, too. Entirely different is the approach of Jiao et al. applying a modified Krätschmer-method to coat Fe, Co and Ni nanopar-

[*] *Prof. Dr. Dieter Vollath,*[+] *Dr. Dorothée V. Szabó*
Forschungszentrum Karlsruhe,
Institut für Materialforschung III
P.O.Box 3640, D-76021 Karlsruhe, Germany
E-mail: dieter.vollath@nanoconsulting.de

[+] *Now with:*
Nano Consulting
Primelweg 3, D-76297 Stutensee, Germany

ticles with amorphous carbon or graphite.[12] Carbon coated Co-nanocapsules have also been prepared by chemical vapour condensation.[13] Sethi and Thölén produced metal nanoparticles by evaporation and condensation and oxidised them partly in a subsequent step resulting in metal particles and the corresponding oxide as shell.[14]

Besides gas phase reactions discussed above, wet chemical methods were developed, too. Coated semiconducting nanoparticles were synthesised by wet chemical ion-exchange reactions.[15] Polymer coated Fe nanoparticles may be prepared by thermal decomposition of an appropriate precursor in the presence of polymer dispersants.[16] Sonochemical methods are another possibility to prepare coated nanoparticles in the size range of ca. 5 15 nm.[17] The sol-gel process is one of the standard methods for preparing nanocomposites consisting of nanoparticles embedded in a matrix. As reported from different authors, the resulting nanocomposites may be of the inorganic/inorganic[18–21] or inorganic/organic[22] type. Similarly, Ziolo et al. applied an in-situ formation method of nanoparticles in ion-exchanging resin to obtain ceramic/polymer nanocomposites.[23]

2. Morphology of Nanocomposites

2.1 Particulate Nanomaterials

Physical properties of nanoparticulate materials usually depend on the volume or the surface of the particles. Therefore, it is absolutely necessary that the particle size distribution is as narrow as possible. Such a narrow size distribution is visible in figure 1 depicting a typical electron micrograph of nanocrystalline zirconia. This micrograph shows nearly spherical particles with a size of ca. 5 nm. Dark field imaging and high-resolution electron microscopy reveal that each particle is a single crystal and free of dislocations or twins. The particle size can be adjusted during synthesis. This is demonstrated in the particle size spectrum determined by particle mass spectrometry[24–28] shown in Figure 2 where the particle size was adjusted to a mean value of 3.1 nm. Smaller particles, down to 2 nm, are possible if one reduces the rate of synthesis significantly. Alumina nanoparticles with sizes below 7 or 8 nm are amorphous and rounded, whereas larger particles are crystalline and faceted.[29] In this case, the particles are crystallised in the γ-phase, indicating a critical diameter for crystallisation of alumina.[29,30]

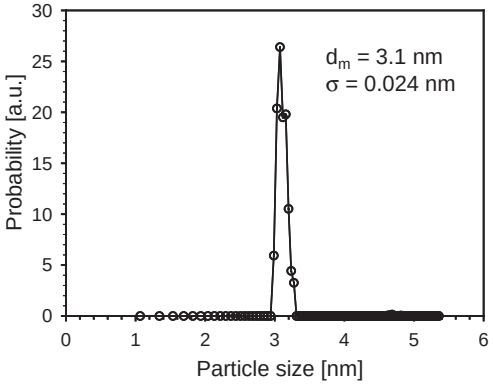

Fig. 2. Particle size distribution of zirconia determined by particle mass spectrometry [24].

As mentioned in the introduction, for nanocomposites, coated nanoparticles are more important than single-phase nanoparticles. In general, the Karlsruhe Microwave Plasma Process is capable to produce three types of nanocomposites in situ:

Ceramic cores coated with a second ceramic phase.[2,7,30]

Ceramic cores coated with a polymer or another organic phase.[8,31]

Ceramic cores decorated with metallic clusters.

Figure 3 shows a typical example of a ceramic/ceramic nanocomposite particle based on the system ZrO_2-Al_2O_3. The system alumina and zirconia is a perfect model for this type of composites, as it fulfils the necessary requirements of not exhibiting mutual solubility and not forming a common compound.[32] The composite particle depicted in Figure 3 con-

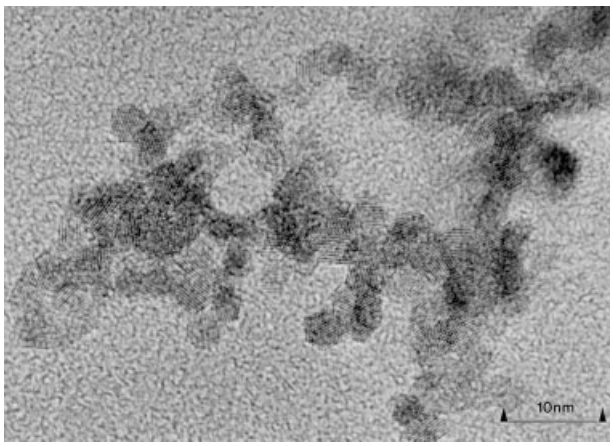

Fig. 1. Electron micrograph of zirconia particles. The particle size is in the range from 3 to 4 nm.

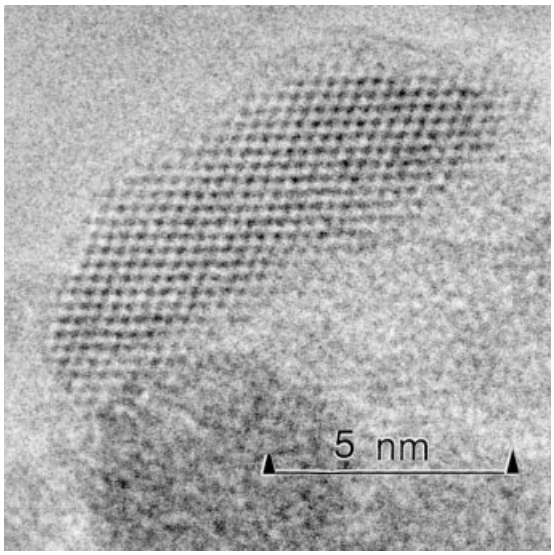

Fig. 3. Crystallised zirconia nanoparticle coated with ca. 0.5 nm glassy alumina.

sists of a crystallised zirconia core, characterised by lattice fringes, and a coating of glassy alumina. The alumina coating is just visible as faint halo with a thickness of ca. 0.5 nm.

Applications of nanomaterials, especially as functional ones, are not connected with severe thermal or mechanical load. Therefore, for most of the applications a polymer used as binder or distance holder between the particles is sufficient. This lead to the use of polymer coated ceramic nanoparticles as starting material. Depending on the surface properties needed for the application, either methacrylic acid (MA), methyl methacrylic acid (MMA), or hydroxy propyl methacrylic acid (HPMA) are used as monomers for polymer coating ceramic nanoparticles. These monomers polymerise under the influence of temperature and uv-radiation originated from the microwave plasma.[8] IR absorption studies revealed that during the PMMA coating process a substantial number of ester groups are transformed into the corresponding carboxylates.[33] In contrast to the pure monomer or polymer, the polymer bond at the surface of the oxide is insoluble in tetrahydrofurane, THF, or any other solvent. Independently of the precursor MAA or MMA, the polymer bond to the surface is modified and is denoted m-PMMA within this paper. Therefore, a nanocomposite particle consisting of a ceramic core and a polymer coating may be described as one molecule like R-(C=O)-O-(oxide particle). This description is in good agreement with earlier findings by Meyer and coworkers.[34] They propose an ester-like linkage between the carboxylic groups and metal surface atoms of oxide such as TiO_2 or SiO_2. Similarly, Weng et al. found surface binding between carboxylic groups and TiO_2 nanoparticles predominantly in ester form.[35] Figure 4 depicts the typical morphology of such a composite particle. In this micrograph, the particle core consists of γ-Fe_2O_3, whereas the coating is made of m-PMMA. Usually, the thickness of the coating is selected to be in the range between 0.5 and 2 nm. For reasons of visibility, for the micrograph the thickness of the coating was selected to be thicker, in the range of approximately 5 nm.

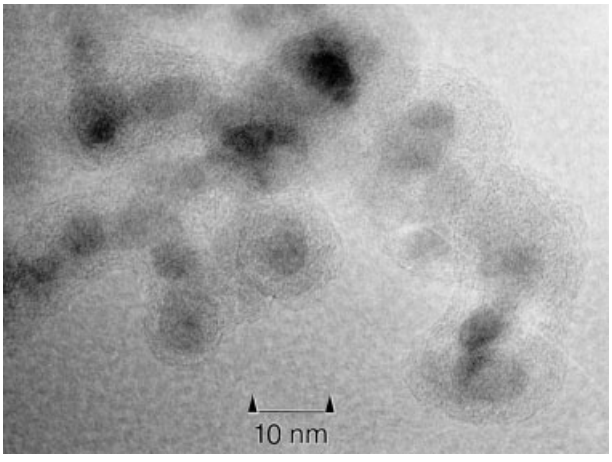

Fig. 4. Maghemite, γ Fe_2O_3 nanoparticles coated with m PMMA. In this figure, it is clearly visible that the particles are individually coated. The cores do not touch each other. The polymer coating is visible as a halo around the darker cores.

2.2 Consolidated Nanocomposites

A consolidation process, as pressing and sintering of alumina coated zirconia kernels, leads to a product with a microstructure as depicted in Figure 5. Because of the small solubility of Zr in Al_2O_3, during sintering, the size of the zirconia particles did not increase significantly. On the other hand, this small solubility leads to zirconium rich areas around the zirconia particles, visible as darker halo around the zirconia particles in the electron micrograph. In any case, it is remarkable that after sintering to full density, the size of the zirconia phase remains to be less than 10 nm.

For ceramic/polymer nanocomposites, the final polymerisation has to be initiated during densification. This is either done by thermal polymerisation of the residual PMMA oligomers or by a polymerisation initiated by the addition of a cross linker.[36] Generally, densification of a ceramic/polymer composite powder, as shown in Figure 5, is performed by hot pressing in the temperature range from 100 to 150 °C. In the case of Al_2O_3/m-PMMA this procedure may lead to transparent bodies. Figure 6 shows the morphology of hot pressed γ-Fe_2O_3/m-PMMA. The specimen for this electron micrograph, a slice with a thickness of 20 nm, was prepared by

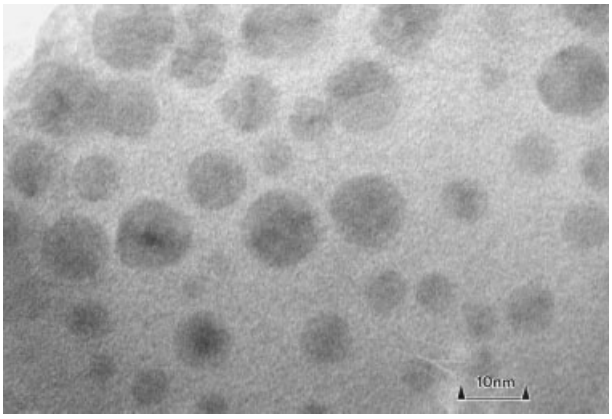

Fig. 5. Sintered ZrO_2/Al_2O_3 nanocomposite. It is remarkable to realise that in spite of the full densification, the size of the zirconia particles did not increase their size signifi cantly during sintering.

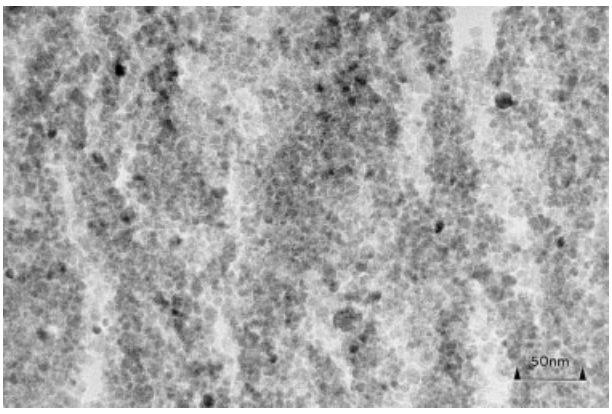

Fig. 6. Morphology of a γ Fe_2O_3/m PMMA body prepared by hot pressing. The speci men is a 20 nm thick section cut with an ultramicrotome. The striation is an artefact from specimen preparation.

mechanical cutting with an ultramicrotome. During this preparation, the specimen broke into small stripes, as it is visible in figure 6. Looking at particle sizes, one realises that all that except one particles are of equal size.

3. Properties of Nanocomposites

3.1 General Considerations

High quality nanocomposites, in special coated nanoparticles, are expensive and highly sophisticated materials. Therefore, it is necessary to search for materials with great gain in properties for high value added applications. These properties may be connected to one of the following phenomena:

Diffusion barrier against grain growth during sintering: Provided the mutual solubility between core and coating is close to nil, the coating may act as diffusion barrier. This may be used to protect the core with its special properties against the influence of the surrounding atmosphere. Such a diffusion barrier thwarts grain growth of the core particles during sintering, whereas the coating material forms larger grains. This situation is already depicted in Figure 5. The protection against the surrounding atmosphere goes along with this phenomenon:

Modification of the chemical surface properties: Such modifications are needed especially in medicine and pharmacology, where luminescent or magnetic nanoparticles are used for identification and quantification of cells and similar structures.[37,38] To attach appropriate ligands with the needed property at the surface of the nanoparticle, it is of great importance to modify the particle surface by coating with a material, well suited to attach specific organic compounds.

New physical properties: Most of the very special properties of nanoparticles are ones of isolated single particles. To maintain these properties it is necessary to reduce the interaction of the particles using a distance holder. Additionally, new physical properties are also possible by exploiting interface phenomena between core and coating. The examples of physical properties explained in the next chapters may be summarised in this class.

3.2 Superparamagnetism

In conventional materials, Bloch walls subdivide the grains into magnetic domains. The size of these magnetic domains is ruled by thermodynamics. Therefore, coercitivity and remanence are largely independent of the grain size. If the grain size is reduced to a point, where the grains are free of Bloch walls, coercitivity and remanence are increasing drastically. This is the size range where each grain is a single domain. This phenomenon is used for magnetic data storage. Further reduction of the grain size leads to a complete vanishing of coercitivity and remanence caused by thermal fluctuations of the vector of magnetisation. The dependency of the remanence or coercitivity on the grain size is shown schematically in figure 7. The superparamagnetic regime is characterised

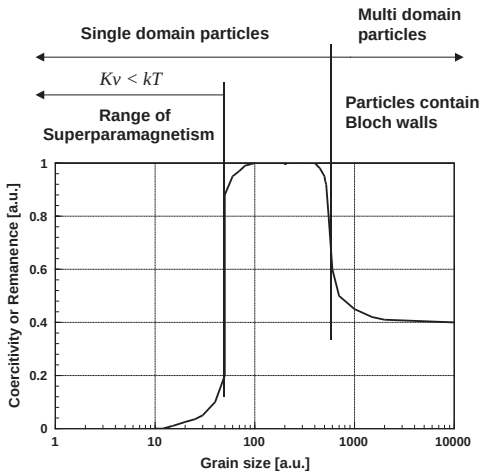

Fig. 7. Dependency of the coercitivity or remanence as a function of the grain size. Ad ditionally, this graph shows the transition of multi domain particle to single domain particles and the second transition to superparamagnetism.

by the fact that the volume dependent energy of magnetic unisotropy $K\nu$ (K ... material constant of magnetic unisotropy, ν ... volume of the particle) keeping the vector of magnetisation in a certain direction is smaller than the thermal energy kT (k ... Boltzmann constant, T ... temperature).

$$K\nu < kT \tag{1}$$

Figure 8 depicts a typical static magnetisation curve of a superparamagnetic ferrite containing 15.3 wt% Fe_2O_3. This composite specimen exhibits a saturation magnetisation of 30 Am^2kg^{-1}. This value is significantly lower than the one found for conventional ferrites. This is, because each ferrite nanoparticle has a surface layer with a thickness of ca. 1 nm not contributing to the magnetisation.

With decreasing energy of unisotropy $K\nu$ the frequency of fluctuation increases. According to Néel,[39] the fluctuation time τ is expressed by:

$$\tau = \tau_0 \exp(K\nu/\lambda Y) \tag{2}$$

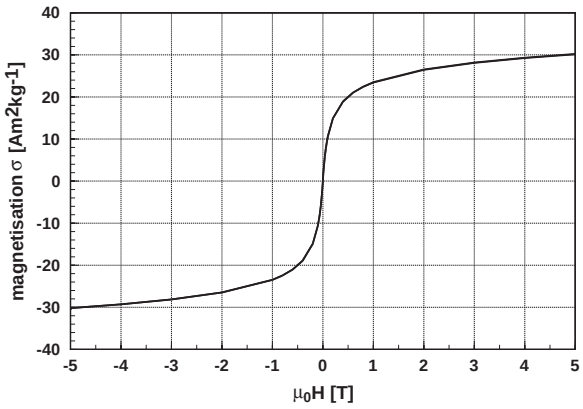

Fig. 8. Static magnetisation curve of γ Fe_2O_3/m PMMA consolidated nanocomposite powder.

τ_0, the relaxation time constant, depends on the material and is in the range from 10^{-8} to 10^{-12} sec. Provided the particles are sufficiently small, the relaxation time τ is smaller than 10^{-9} sec. These considerations are valid for one single isolated particle or a set of non-interacting ones. In consolidated parts, superparamagnetism is preserved by reduction of the magnetic interaction using a distance holder. The dependency of the magnetisation M of n non-interacting superparamagnetic particles as function of the field H at the temperature T is described with sufficient good approximation by the Langevin function $L(m,H,T)$:

$$M = nmL(m,H,T) = nm(cth(\frac{mH}{kT}) - \frac{kT}{mH}) \quad (3)$$

This relationship may also be used to calculate the particle size distribution from the magnetisation curve. To do this, one assumes I classes each with n_i particles of the moment m_i. With these assumptions, the magnetisation curve may be fitted by:

$$M = \sum_{i=1}^{I} n_i m_i L(m_i,H,T) \quad (4)$$

Figure 9a depicts the distribution of magnetic moments derived from the magnetisation curve in Figure 8. To estimate the particle size distribution, one has to consider that the magnetic moments m_i are proportional to the volume of the particle. To obtain the particle size distribution one has to normalise the distribution of moments with $(m_i)^{0.333}$. The resulting distribution function is shown in Figure 9b. To obtain sizes in nm, one has to calibrate this distribution function with electron microscopy images. This is, because nanoparticles have a boundary layer of ca. 1 nm with reduced magnetic properties.

Literature values of the saturation magnetisation for superparamagnetic nanocomposites vary dramatically. Ziolo et al. determined 15 Am^2kg^{-1} at 1 T and 300 K for a Fe_2O_3/polymer composite with 21.8 wt% of Fe_2O_3.[23] Nanocomposites containing 30 wt% of $ZnFe_2O_4$ in a silica matrix show at 5 T a saturation magnetisation of 12.6 Am^2kg^{-1} measured at 78 K.[40] Savii et al. found 8.04 Am^2kg^{-1} at 0.216 T for Fe_2O_3-SiO_2 nanocomposites containing 25 wt% Fe_2O_3.[20] Compared to the magnetic moments obtained with γ-Fe_2O_3/m-PMMA nanocomposites depicted in figure 8, these values are quite small.

The static magnetisation curves shown until now were measured in a system with a time constant of 100 sec. For applications, shorter time constants are essential. Therefore, figure 10 depicts the susceptibility of different ferrites made of pressed ferrite/m-PMMA nanocomposites in comparison with a commercial conventional ferrite. One realises that the susceptibility values are in the same range. Relaxation times

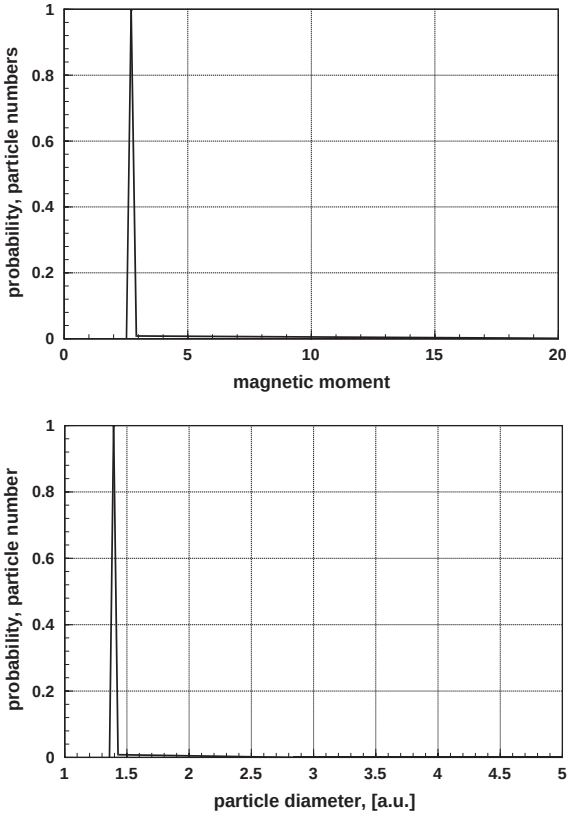

Fig. 9. (a) Distribution of magnetic moments of m PMMA coated γ Fe_2O_3derived from the magnetisation curve shown in Figure 8. (b) Particle size distribution of PMMA coated γ Fe_2O_3derived from the distribution of magnetic moments shown in (a).

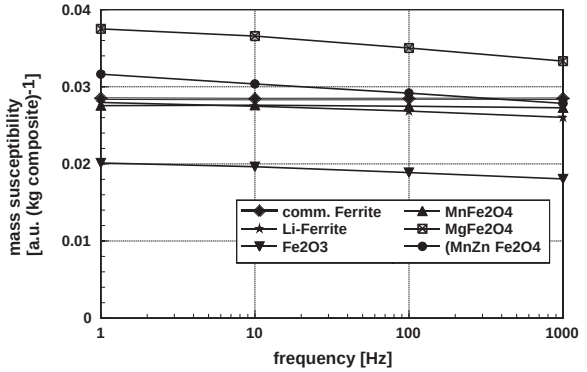

Fig. 10. Mass susceptibility of different ferrite/polymer nanocomposites in comparison to a commercially available ferrite.

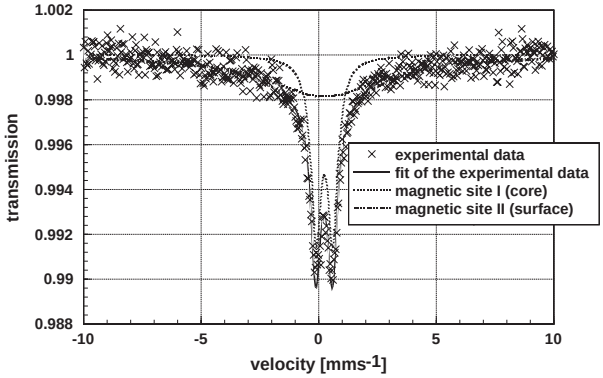

Fig. 11. Mößbauer spectrum of a γ Fe_2O_3/ZrO_2 composite specimen. The experimental data are composed of the spectra of the magnetic core and the non magnetic surface layer.

of less than one ns are interesting for technical applications in future. The ultimate proof for those short relaxation times is the Mößbauer effect. This spectroscopy compares the relaxation frequencies with the Lamor frequency of the iron nucleus. Provided the relaxation frequency is the higher one, the iron nuclei "do not realise" that there is a high magnetic crystal field. This leads to Mößbauer spectra showing the quadrupole doublet of non-magnetic material instead of the sextette observed with magnetic materials. Figure 11 shows this for a γ-Fe_2O_3/ZrO_2 composite specimen. This Mößbauer spectrum is a superposition of two spectra: one of the ferrimagnetic core and one of the boundary layer. In the example given in Figure 11, the volume ratio of magnetic core over outer boundary layer is 0.72. This reduced volume of ferrimagnetic material in γ-Fe_2O_3 leads to the well-known reduction of the saturation magnetisation and susceptibility. In spite of these problems, the susceptibility of superparamagnetic composites is in the range as it is found in conventional ferrites. This is well visible in Figure 10.

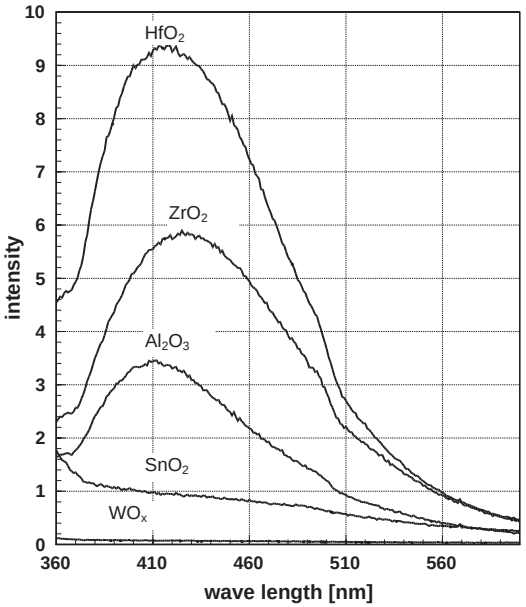

Fig. 12. Luminescence of different oxide nanoparticles as powder coated with m PM MA.

3.3 Luminescence

Generally, luminescence is observed with aromatic organic molecules. Quite often, these molecules exhibit limited stability and toxicity. Therefore, luminescence properties are sought in the field of inorganic nanoparticles. Until now, the most important luminescent nanoparticles are semiconducting nanoparticles. In this class of materials, quantum dots based on sulphides, selenides, or tellurides of zinc and cadmium[41,42] or GaN[43,44] show the best luminescence efficiency. Doping may increase the efficiency of light emission; typical examples are ZnS[45] and CdSe.[46] Particles based on Cd, Se, and As are as well toxic as carcinogenic. Therefore, the need of non-toxic luminescent nanoparticles leads to broad research activities mainly in the direction of rare earth doped oxide nanoparticles.[47] On air, the surface of oxide nanoparticles, such as zinc oxide, form a hydroxide layer quenching luminescence. Coating of the surface of the particles with a polymer protects the oxide surface against ambient air, even against water.[48,49]

It was discovered that wide gap insulating oxides exhibit luminescence when coated with m-PMMA.[49] This is shown in Figure 12 depicting the luminescence of different oxide nanoparticle powder specimen coated with m-PMMA. It is obvious, nanoparticles of HfO_2, a wide band insulator, exhibit the highest and nanoparticles of WO_x, a semi-conductor, the lowest luminescence intensity. Nanocomposites with γ-Fe_2O_3 core never show luminescence at all. The particle size of the ceramic cores was in the range of 5 nm. For the wide band insulating oxide cores HfO_2, ZrO_2, and Al_2O_3, the luminescence intensity increases with the uv absorption in the ceramic core. Figure 13 is a graph showing the luminescence intensity of powders of these nanoparticles as a function of the absorbance for the 325 nm excitation line in an aqueous suspension. In contrast to the intensity, the wavelength of the luminescence intensity maximum does not depend on the oxide core. The small differences visible in Figure 12 are probably caused by differences in the particle size.

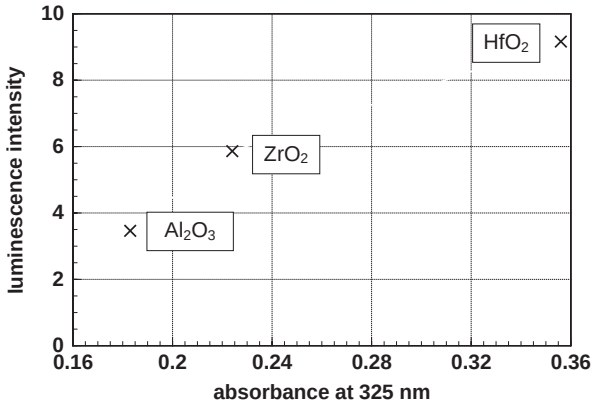

Fig. 13. Luminescence intensity of the highly insulating oxides HfO_2, ZrO_2, and Al_2O_3 as function of the absorbance of the powder suspended in water with a concentration of 0.01 gl ^{1}.

It may be astonishing that combinations of two non-luminescent materials exhibit relatively strong luminescence in a composite. Therefore, experiments to clarify this phenomenon were performed. Starting point were the findings that during the PMMA coating process a substantial number of ester groups have formed an ester-like linkage between the carboxylic groups and metal surface atoms of oxide.[33] Therefore, these composite particles form molecule-like structures of the type R-(C=O)-O-(oxide particle). Combining these findings with the experimental result that the luminescence intensity increases with increasing uv absorption in the ceramic core, leads to the assumption that the observed luminescence phenomena are related to an absorption process in the ceramic core and a transfer of excitation via the carboxylate bonds

to the polymer coating. The modified PMMA is characterised by a carbonyl group directly adjacent to the oxide surface. Carbonyl groups are responsible for luminescence in aliphatic compounds[50] as it is known from e.g. biacetyl, CH_3-(C=O)-(C=O)-CH_3. To prove this postulated correlation, formic acid ethyl ester (FAME), H-(C=O)-O-CH_3, showing luminescence in the range between 360 and 410 nm when dissolved in water, was selected as precursor to coat the oxide particles. This leads to the smallest possible molecule H-(C=O)-O-(oxide particle) containing a carbonyl group at the oxide surface. Additionally, samples made of ZrO_2 nanoparticles coated by diethylether (DEE), C_2H_5-O-C_2H_5, as precursor were prepared to form molecules like C_2H_5-O-(ZrO_2). This material does not contain any carbonyl group. At the outside, both types of specimen were coated with PHPMA. This polymer was selected because oxide particles coated with PHPMA show only very week luminescence. In this case there is a high probability that the $(OH)^-$ groups are bond directly to the surface. Figure 14 exhibits the luminescence spectra of these specimens. It is obvious that FAME as precursor for coating leads to identical spectra as found with m-PMMA coating, whereas the coating without carbonyl group leads to an entirely different spectrum. This is a clear proof that the carbonyl group at the particle surface is responsible for luminescence of these nanocomposites.

To shed more light at the mechanism, the size dependency of the luminescence intensity and wavelength was determined. For these experiments, ZrO_2/m-PMMA was taken as example. The particle size was estimated with a precision of ca. ± 0.2 nm by evaluation of x-ray diffraction line profiles using the Scherrer formula.[51] These experiments resulted in three correlations:

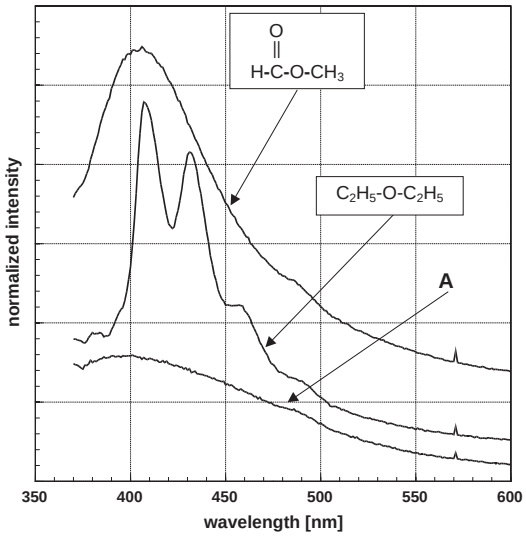

*Fig. 14. Luminescence spectrum of nanocomposite powders with ZrO_2 kernels coated with FAME and DEE. The outside of the composites is coated with PHPMA. The spectra are characterised by the monomer. Additionally, the weak emission spectrum of ZrO_2 coated with PHPMA (**A**) is given for comparison. The spectra are normalised and stacked.*

The peak luminescence intensity increases with decreasing particle diameter following the law:

$$I = I_0 + b/d \tag{5}$$

(I ... intensity, I_0 = 2.04 ± 0.1, b = 20.8 ± 0.1 nm ... constants, and d ... particle diameter in nm). As for a given amount of material, the number of particles is proportional d^{-3} and the surface of one particle is proportional d^2 a dependency of d^{-1} describes a direct proportionality to the total surface of the particles. Therefore, the proportionality of the intensity with d^{-1} correlates the emission mechanism with the particle surface.

Decreasing particle size goes parallel with a blue shift described by

$$1/\lambda = 1/\lambda_0 + bd^3 \tag{6}$$

(λ_0 = 416.5 ± 0.05 nm, b = 1.061 × 10^{-6} ± 5 × 10^{-9} nm^{-4}). Figure 15 depicts the experimental data. This blue shift goes parallel with a reduction of the line width.

The line width at half intensity follows the relation

$$\Delta E = \Delta(1/\lambda) = \Delta E_0(1 - \exp(-bd)) \tag{7}$$

(ΔE_0 = 5.73*10^{-4} ± 1.6*10^{-6} nm^{-1}, b = *6.39*10^{-1} ± 5.8*10^{-3} nm). A fit of equal precision is obtained using the function:

$$\Delta E = \Delta(1/\lambda) = \Delta E_0 - b/d \tag{8}$$

(ΔE_0 = 6.43*10^{-4} ± 2.2*10^{-6} nm^{-1}, b = 4.59*10^{-4} ± 3*10^{-6}).

The latter two relations connect the emitted light directly to the band structure of the ceramic core. This finding corresponds well with the result that the uv-quanta are absorbed in the ceramic core followed by a transfer of the excitation to the carbonyl group bond at the surface.

The interaction of the m-PMMA coating with the oxide core is different in the case of a semi-conducting oxide exhibiting luminescence. ZnO is representative for these materials.

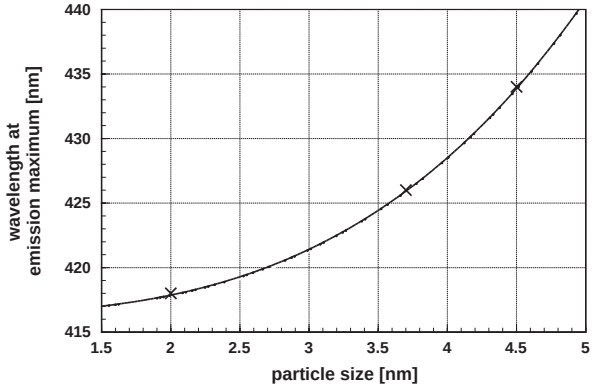

Fig. 15. Wavelength of the emission maximum as a function of the particle size of ZrO_2/m PMMA nanoparticles determined at the maximum of the intensity. The experimentally found blue shift with decreasing particle size is fitted by $1/\lambda = 1/\lambda_0 + bd^3$.

Luminescence spectra of ZnO/m-PMMA nanocomposites with varying size of the oxide are shown in figure. Typical for these composites is a broad emission consisting of two broad overlapping lines. Determination of the particle size by x-ray diffraction is impossible because of the overlapping lines. Therefore, the particle size was determined with reduced precision, estimated to be ca. ± 3 nm, by electron microscopy. Fujihara et al. found on ZnO particles with a size of 6.2 nm embedded in MgF_2 films a similar splitting of the emission.[52] This suggests that the splitting is a consequence of the interaction of the ZnO particles with the surrounding material. For ZnO/m-PMMA, both of the overlapping luminescence peaks exhibit blue shift with decreasing particle size. Additionally, the intensity ratio peak 1 over peak 2 increases with decreasing particle size. These experimental findings follow the relation:

$$I_2/I_1 = A + kd^{-2} \tag{9}$$

(I_2, I_1 = Intensity of the second or first peak, respectively, A=1.120 ± 2×10^{-4} and k = 4.9 ± 5*10^{-3} nm^{-2}). Assuming oxide polymer interaction as source for peak 1 the intensity of peak 1 should be proportional d^{-1}. Therefore, the intensity of peak 2 is

$$d^{-2}d^{-1} = d^{-3} \tag{10}$$

This is exactly the proportionality expected in quantum confinement systems. Because of the overlapping, it is difficult to analyse the blue shift of the first peak with sufficient precision. The blue shift of the second peak is described by the expression:

$$1/\lambda = 1/\lambda_0 + bd^{-3} \tag{11}$$

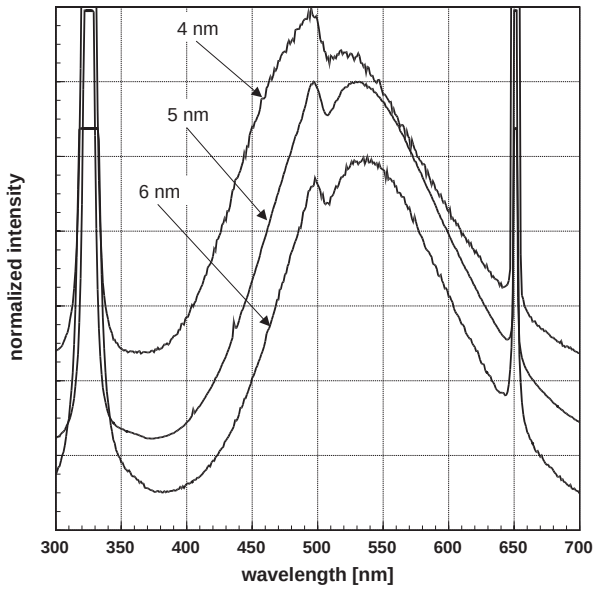

Fig. 16. Emission spectra of ZnO/m PMMA nanocomposites, influenced by the parti cle size. Additionally, the spectra show the exciting line in first order at 325 nm and at 650 nm in second order. The spectra are stacked and normalised.

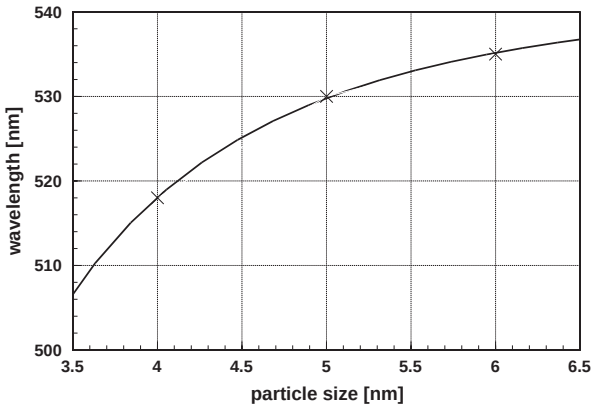

Fig. 17. Influence of the particle size on the blue shift of the ZnO emission line with decreasing particle size. The experimental points were fitted with $1/\lambda = 1/\lambda_0 + b*d^{-3}$.

(λ_0 = 542.7 ± 0.4 nm, b = 5.61*10^{-3} ± 1*10^{-4} nm^{-2}). The experimental data connected with the fitted function are depicted in Figure 17. The exponent 3, related to quantum confinement, is the same as it was found by Monticone et al. for the blue shift in ZnO.[53]

As the range of colours found with the oxide/m-PMMA nanocomposites is limited, a new type of luminescent nanocomposites was designed.[54] This new composite consists of a ceramic core, a monomolecular layer of an organic lumophore, and a polymer coating for protection and adjusting the surface properties according to the demands. One may expect the following advantages from this new type of composites:

Broad range of possible colours based on the vast amount of commercially available lumophors.

Modification of excitation and emission by the ceramic core.

Combination of different properties by selecting appropriate core and coating materials and

adjustment of the surface properties by selecting a polymer according to the demands.

As a first example of the luminescence spectra a series of composites with different insulating oxide cores, pyrene as lumophore and PMMA as protection coating is shown. Figure 18 reveals that the spectra are independent of the ceramic core, whereas the intensities depend strongly on the ceramic

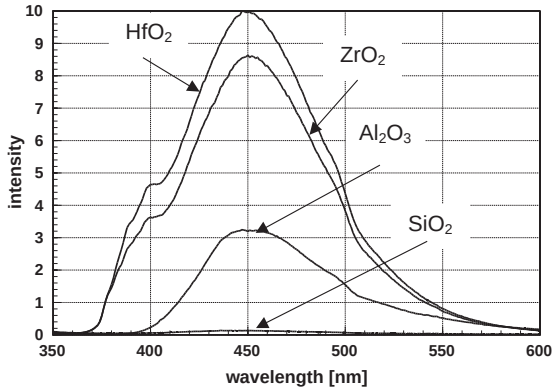

Fig. 18. Luminescence spectra of different oxide/pyrene/PMMA nanocomposites as powder.

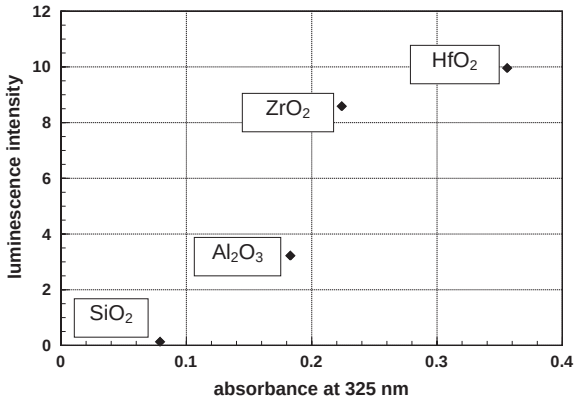

Fig. 19. Luminescence intensity of oxide/pyrene/PMMA nanocomposite particles plotted as function of the absorbance at 325 nm. Absorbance was determined in an aqueous suspension with 0.01 vol% particles in water.

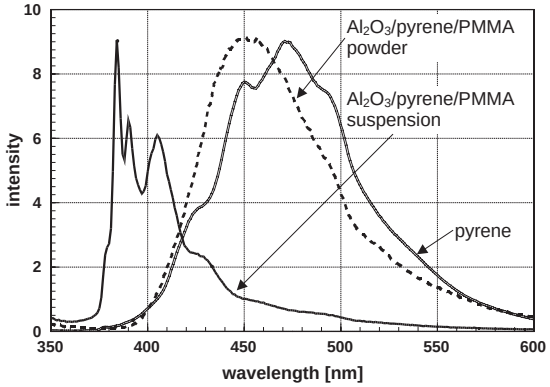

Fig. 21. Comparison of luminescence spectra of solid pyrene, Al_2O_3/pyrene/PMMA nanocomposite as powder and Al_2O_3/pyrene/PMMA suspended in methanol.

core. This spectrum is nearly the same as it is found for pure solid pyrene. Similar as in the case of oxide/m-PMMA nanocomposites, composites with hafnia core exhibit the highest; those with silica core the lowest luminescence intensity. This relationship is also reflected in the absorption of 325 nm uv-quanta used for excitation. As it is demonstrated in Figure 19 the composites with hafnia kernel show the highest, the ones with silica core the lowest absorption. This relationship leads to the assumption that, at an excitation of 325 nm, the uv-quanta are absorbed in the ceramic core. This excitation is transferred to the lumophore molecules at the surface of the composites. As there is no bonding between the ceramic core and the lumophore, one may assume an excitation transfer by dipole interaction such as the Förster mechanism.[55,56] The spectra are changing from the excitonic ones to the molecule spectra in the case that the particle surface is not covered completely. This is demonstrated in Figure 20. Similarly, the transition from the excitonic spectrum to the molecule spectrum is found also in very thin suspensions. For comparison, Figure 21 displays the spectrum of an alumina/pyrene/PMMA composite as powder and suspended in methanol. In this graph, one realises that in a thin suspension, these nanocomposite particles behave like molecules. Obviously, lumophore molecules attached on one nanoparticle are not interacting with each other. This is insofar astonishing as the size relations between the lumophore molecules and the oxide particle are so that the angles between the axes of the molecules are not only 90 ° and 180 °. Therefore, one would have expected at least some interaction between the lumophore molecules on the surface of one ceramic nanoparticle.

In case of oxide particle/pyrene, the emission spectra of pyrene is only very little influenced by oxide core. This is different if one uses anthracene as lumophore. Figure 22 displays the emission spectra of pure anthracene and a Fe_2O_3/anthracene/PMMA nanocomposite. This comparison shows two spectra that are identical except for the most intense line. In the composite, the line at 420 nm is not fitting into the well-known system of vibration modes of anthracene. This extra line is observed independently of the oxide used as core material.

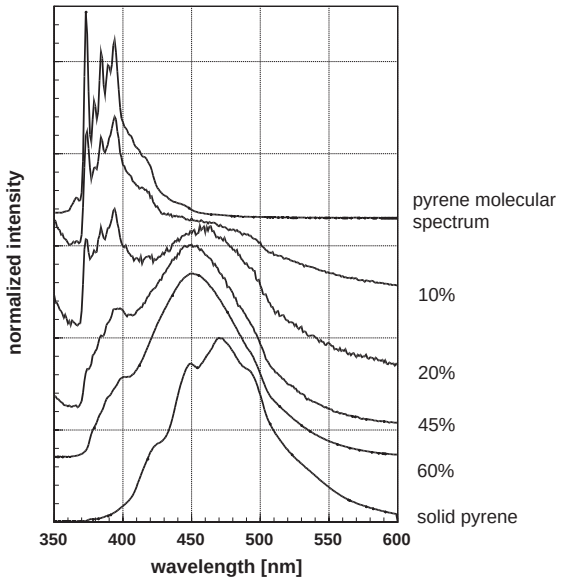

Fig. 20. Luminescence spectra of ZrO_2/pyrene/PMMA nanoparticles with different coverage of the nanoparticle surface with the lumophore. The numbers at the lines indicate the percentage of surface covering. In all cases, the intensity is normalised and the graphs are stacked. For comparison, the emission spectrum of the solid pure lumophore is displayed.

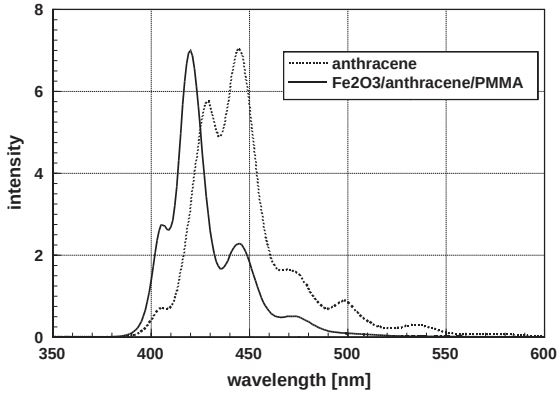

Fig. 22. Emission spectra of pure solid anthracene in comparison with a γ Fe_2O_3/anthracene/PMMA nanocomposite powder.

4. Conclusions

Nanoparticles produced by the Karlsruhe Microwave Plasma Process exhibit a very narrow particle size distribution. This makes them ideal for any application as functional material, as many of the interesting physical properties are volume dependent. As the interaction of the particles changes or even quenches the interesting physical properties, it is necessary to coat each particle either with a second ceramic or organic material. It has been shown that superparamagnetism, a property typical for nanosized ferrites, can be saved into pressed and sintered compacts, provided each individual particle is coated with a distance holder. Applying a second phase as "distance holder" also avoids grain growth during sintering.

In special cases, the interaction between ceramic core and organic coating may lead to new properties. A typical example is luminescence. It was found that carbonyl groups bond to the oxide core exhibit strong luminescence. This luminescence depends strongly on the particle size. It shows blue shift and narrowing of the emission line with decreasing particle size indicating a direct connection between the molecular orbital and the energy bands of the ceramic particle. To broaden the range of possibilities, a second type of luminescent nanoparticles was developed. In this case, a monolayer of lumophore molecules was placed between the ceramic core and the outer polymer layer. Even in this case, without chemical bonding, there are distinct interactions between the ceramic core and the lumophore molecules. Most interesting, lumophore molecules sitting on one particle are not interacting. Such a nanocomposite behaves like one molecule. Similar as in the case of chemically bond molecules at the surface, the uv-quanta for excitation are absorbed on the ceramic core and the excitation is transferred to the luminescent molecules at the surface.

The ceramic core may be selected in a way that it contributes with its own physical property to the properties of a composite. A typical example for such a combination is a superparamagnetic core and a luminescent coating. Materials exhibiting this combination of properties are sought in biotechnology for cell separation and quantification.

5. Experimental Section

The ceramic nanoparticles and ceramic/ceramic or ceramic/organic nanocomposites used in this study, are synthesized using the Karlsruhe Microwave Plasma Process, well suited to produce ceramic nanoparticles coated individually with a ceramic[2,7] or a polymer[8] layer. This is possible, because the particles leave the reaction zone, where the particles are formed, with electric charges of equal sign. As these charged particles repel each other agglomeration is avoided and coating of the particles in subsequent steps of a cascaded process is possible. Depending on the demands, the particle size is adjusted in the range between 3 and 10 nm; in special cases, sizes down to 2 nm are possible. To synthesize the ceramic cores, water-free, volatile precursors, such as Aluminumtrichloride, $AlCl_3$, Zirconiumtetrachloride, $ZrCl_4$, ironpentacarbonyl, $Fe(CO)_5$ or Hafnium-t-butoxide, $Hf[OC(CH_3)_3]_4$ are used. They are introduced as a vapour into the reaction tube just before the reaction zone. These compounds react with the reaction gas, a mixture of Ar and 20 vol% O_2, to the desired nanoparticles. Coating of the ceramic nanoparticles with organic materials is possible, because the temperatures in the system can be kept sufficiently low. This is one of the inherent advantages of microwave plasma processing. The selection of the polymer for the outer layer follows the demands of the application. In general, PMMA is used for coating. For hydrophilic coating PHPMA (poly hydroxy propyl methacrylate) is selected. In the case of PMMA coating, the monomer reacts via carboxylate groups with the oxide surface.[33] In all of these cases, polymerisation is initiated by the uv-radiation from the microwave plasma.[8] Electron microscopy was performed with a Philips CM 30ST. Magnetization was measured using a superconducting SQUID magnetometer. Mößbauer experiments were performed with a Co^{57} source at room temperature. Luminescence spectra were analysed using a spectrometer with Czeney-Turner monochromator. For excitation, a HeCd laser (325 nm) connected to a monochromator was used. The optical signal was detected with a photomultiplier tube. Absorption measurements were done in diluted suspensions of nanopowders in the transmission mode.

[1] H. Gleiter, *Prog. Mat. Science*, **1989**, *33*, 223.
[2] D. Vollath, *German Patent DE9403581U1*, **1994**.
[3] D. Vollath, K. E. Sickafus, R. Varma, In *Mat. Res. Soc. Symp. Proc.* **1992**, *269*, 379.
[4] D. Vollath, K. E. Sickafus, *Nanostruct. Mater.* **1992**, *1*, 427.
[5] D. Vollath, K. E. Sickafus, *J. Mater. Res.* **1993**, *8*, 2978.
[6] D. Vollath, K. E. Sickafus, *Nanostructured Materials* **1993**, *2*, 451.
[7] D. Vollath, D. V. Szabó, *Nanostructured Materials* **1994**, *4*, 927.
[8] D. Vollath, D. V. Szabó, B. Seith, *German Patent DE196 38 601C1*, **1996.**
[9] W. Chang, G. Skandan, H. Hahn, S. C. Danforth, B. H. Kear, *Nanostructured Materials* **1994**, *4*, 345.
[10] C. H. Hung, J. L. Katz, *J. Mater. Res.* **1992**, *7*, 1861.
[11] C. H. Hung, J. L. Katz, *J. Mater. Res.* **1992**, *7*, 1870.
[12] J. Jiao, S. Seraphin, X. Wang, J. C. Whitters, *J. Appl. Phys.* **1996**, *80*, 103.
[13] Z. H. Wang, C. J. Choi, B. K. Kim, J. C. Kim, Z. D. Zhanh, *Carbon* **2003**, *41*, 1751.
[14] S. A. Sethi, A. R. Thölén, *Nanostructured Materials* **1993**, *2*, 615.

[15] H. S. Zhou, I. Honma, J. W. Haus, H. Sasabe, H. Komiyama, *J. Luminescence* **1996**, *70*, 21.
[16] N. A. D. Burke, H. D. H Stöver, F. P. Dawson, J. D. Lavers, P. K. Jain, H. Oka, *IEEE Transactions on Magnetics* **2001**, *37*, 2660.
[17] K. V. P. M. Shafi, A. Ulman, X. Yan, N.-L. Yang, C. Estournès, H. White, M. Rafailovich, *Langmuir* **2001**, *17*, 5093.
[18] S. Komarneni, *J. Mat. Chem.* **1992**, *2*, 1219.
[19] J. Plocek, A. Hutlova, D. Niznansky, J. Bursik, J.-L. Rehspringer, Z. Micka, *J. Non-Cryst. Solids* **2003**, *315*, 70.
[20] C. Savii, M. Popovici, C. Enache, J. Subrt, D. Niznansky, S. Bakardzieva, C. Caizer, I. Hrianca, *Solid State Ionics* **2002**, *151*, 219.
[21] E. M. Moreno, M. Zayat, M. P. Morales, C. J. Serna, A. Roig, D. Levy, *Langmuir* **2002**, *18*, 4972.
[22] H. Schmidt, *Macromol. Symp.* **2000**, *159*, 43.
[23] R. F. Ziolo, E. P. Giannelis, B. A. Weinstein, M. P. O'Horo, B. N. Ganguly, V. Mehrotra, M. W. Russell, D. R. Huffman, *Science* **1992**, *257*, 219.
[24] P. Roth, private communication, **2000**.
[25] A. Hospital, P. Roth, *23rd Symposium (International) on Combustion*, The Combustion Institute, Pittsburgh, PA, **1990**, 1573.
[26] P. Roth, A. Hospital, *24th Symposium (International) on Combustion*, The Combustion Institute, Pittsburgh, PA, **1992**, 981.
[27] P. Roth, A. Hospital, *J. Aerosol Science* **1994**, *25*, 61.
[28] D. Lindackers, M. G. D. Strecker, P. Roth, C. Janzen, S. E. Pratsinis, *Combust. Sci. and Tech.* **1997**, *123*, 287.
[29] D. Vollath, *KfK-Nachrichten* **1993**, *25*, 139.
[30] D. Vollath, D. V. Szabó, J. Haußelt, *J. Europ. Ceram. Soc.* **1997**, *17*, 1317.
[31] D. Vollath, D. V. Szabó, J. Fuchs, *Nanostructured Materials* **1996**, *12*, 433.
[32] The American Ceramic Society, *Phase Diagrams for Ceramists*, Westerville, OH, USA **1975**, 135.
[33] I. Lamparth, D. V. Szabó, D. Vollath, *Macromolecular Symposia* **2002**, *181*, 107.
[34] T. J. Meyer et al., *Inorg. Chem.* **1994**, *33*, 3952.
[35] Y.-X. Weng, L. Li, Y. Liu, L. Wang, G.-Z. Yang, *J. Phys. Chem. B* **2003**, *107*, 4356.
[36] I. Lamparth, *German patent application DE 101 44993.3*, **2001**.
[37] D. Pfefferer, S. Wagner, M. Kresse, M. Taupitz, W. Ebert, *ECR '95, Wien (A),05.-10.03.95*
[38] A. Jordan, P. Wust, H. Fähling, W. Jahn, A. Hinz, R. Felix, *Int. J. Hyperthermia* **1993**, *9*, 51.
[39] L. Néel, *Comt. Rend*. **1949**, *228*, 664.
[40] Z. H. Zhou, J. M. Xue, H. S. O. Chan, J. Wang, *Materials Chemistry and Physics* **2002**, *75*, 181.
[41] Y. Tian, T. Newton, N. A. Kotov, D. M. Guldi, J. H. Fendler, *J. Phys. Chem.* **1996**, *100*, 8927.
[42] H. E. Porteanu, E. Lifshitz, M. Pflughoefft, A. Eychmüller, H. Weller, *Phys. Stat. Sol. B* **2001**, *226*, 219.
[43] Y. Yang, V. J. Leppert, S. H. Risbud, B. Twamely, P. P. Power, H. W. H. Lee, *Appl. Phys. Lett.* **1999**, *74*, 2262.
[44] Y. G. Cao, X. L. Chen, J. Y. Li, Y. C. Lan, J. K. Liang, *Appl. Phys. A* **2000**, *71*, 229.
[45] P. Yang, M. Lu, D. Xu, D. Yuan, G. Zhou, *Appl. Phys. A* **2001**, *73*, 455.
[46] F. V. Mikulec, M. Kuno, M. Bennati, D. A. Hall, R. G. Griffin, M. G. Bawendi, *J. Am. Chem. Soc*. **2000**, *122*, 2532.
[47] Y. Wang, H. Cheng, L. Zhang, Y. Hao, J. Ma, B. Xu, W. Li, *J. Mol. Catal. A: Chem*. **2000**, *151*, 205.
[48] D. Vollath, *German patent application*, *DE 101 54988.A1*, **2001**.
[49] D. Vollath, I. Lamparth, D. V. Szabó, *Mat. Res. Soc. Symp. Proc.* **2002**, *703*, V7.8.1.
[50] C. A. Parker, in *Photoluminescence of Solutions* Elsevier, Amsterdam **1968**, p. 21
[51] P. Scherrer, *Göttinger Nachrichten, Math. Phys*. **1918**, 98.
[52] S. Fujihara, H. Naito, T. Kimura, *Thin Solid Films* **2001**, *389*, 227.
[53] S. Monticone, R. Tufeu, A. V. Kanaev, *J. Phys. Chem. B* **1998**, *102*, 2854.
[54] D. Vollath, I. Lamparth, F. Wacker, *German patent application DE 102 03907A1*, **2002**.
[55] V. T. Förster, *Ann. Phys*. **1948**, *6*, 54.
[56] V. T. Förster, *Naturwissenschaften* **1948**, *33*, 93.